Journal of
Synchrotron Radiation

ISSN 0909-0495

Received 16 February 2009
Accepted 27 July 2009

Spatial structure of a focused X-ray beam diffracted from crystals

A. Kazimirov,[a]* V. G. Kohn,[b] A. Snigirev[c] and I. Snigireva[c]

[a]Cornell High Energy Synchrotron Source (CHESS), Cornell University, Ithaca, NY 14853, USA, [b]Russian Research Center 'Kurchatov Institute', 123182 Moscow, Russia, and [c]European Synchrotron Radiation Facility, BP 220, 38043 Grenoble, France. E-mail: ayk7@cornell.edu

The spatial structure of a beam focused by a planar refractive lens and Bragg diffracted from perfect silicon crystals was experimentally studied at the focal plane using a knife-edge scan and a high-resolution CCD camera. The use of refractive lenses allowed for a detailed comparison with theory. It was shown that diffraction leads to broadening of the focused beam owing to the extinction effect and, for a sufficiently thin crystal, to the appearance of a second peak owing to reflection from the back surface. It was found that the spatial structure of the diffracted beam depends on whether the crystal diffracts strongly (dynamically) or weakly (kinematically). The results help to understand the physical origin of the diffracted intensity recorded in a typical microbeam diffraction experiment.

Keywords: X-rays; focusing; refractive lenses; X-ray diffraction; extinction effect.

1. Introduction

Theoretical analysis of the Bragg diffraction of a very narrow X-ray beam by a crystal performed in the early 1970s (Afanas'ev & Kohn, 1971; Uragami, 1970) revealed interesting phenomena. It was found that the beam originating from the infinitely narrow slit placed on the surface of the crystal is reflected from a thin layer near the top (entrance) surface and from the bottom surface of the crystal. A detector placed at the same entrance surface (a situation hardly realised in a real experiment) would see the diffracted intensity as two separate peaks. The lattice in the bulk does not reflect X-rays. Recently (Kohn, 2006; Kohn & Kazimirov, 2007), this effect was explained in terms of a plane wave expansion of the incident beam. The plane waves inside the angular region of the total reflection are reflected within the extinction length and leave the crystal. Other plane waves are reflected so that for these the depth of reflection is very shallow and inversely proportional to the angular deviation from the Bragg condition. These waves still pass through the bulk of the crystal but do not reflect owing to destructive interference between the waves scattered from various depths. The bottom surface partially breaks this destructive interference and the reflection takes place again.

A new approach to experimentally observe these phenomena was proposed (Kohn, 2006; Kohn & Kazimirov, 2007) based on using focusing optics such as refractive lenses (Snigirev *et al.*, 1996) or Fresnel zone plates (Michette, 1986) to produce a narrow beam, thus eliminating the need for a narrow slit. Moreover, since for a perfect crystal a symmetric Bragg reflection is equivalent to reflection from a mirror, the detector can be placed at the focus and the crystal anywhere between the lens and the detector.

It was shown (Kohn & Kazimirov, 2007) that not only the bottom surface but any structural non-uniformity inside the crystal such as defects or interfaces can break up the destructive interference and show up as regions of additional intensity, thus providing the basis for a new diffraction depth-sensitive imaging technique. First experiments performed using Fresnel zone plates as focusing optics (Kazimirov *et al.*, 2008, 2009) successfully confirmed these ideas by applying the new technique to a study of the local structure of strained silicon-on-insulator layers.

The purpose of this work is a detailed comparison of theory with experiment using perfect silicon crystals of different thickness as model samples and refractive lenses as focusing optics. Refractive lenses offer here significant advantages over other types of focusing optics for several reasons. First, for a refractive lens, the propagator can be written analytically (Kohn, 2003) and, in a thin-lens approximation, which is sufficient for our purpose and will be used in this work, as a simple exponential function. Second, refractive lenses do not require any additional elements such as a beam-stop and an order-sorting aperture, making both the experimental set-up and theoretical simulations more simple and reliable. Two experimental techniques were utilized to measure diffraction patterns: a knife-edge technique and use of a high-resolution CCD camera. The article is organized as follows. In the next section the experimental set-up is shown and the formation of the diffraction pattern is analyzed theoretically. In §3 we will present experimental results obtained from a thick silicon crystal using a knife-edge scan and from thin silicon crystals

using a CCD camera. The experimental results and their interpretation will be discussed in §4, followed by conclusions and outlook.

2. Theory

Let us consider the experimental set-up shown in Fig. 1. An X-ray wave originating from a source of finite transverse size located far upstream from the set-up is restricted by the slit (S) and incident on the compound refractive lens (CRL). We use a paraxial approximation in which the surface of the constant phase has a parabolic shape and two transversal dependences are transformed independently during the wave transport along the direction of propagation. Since the lens and the crystal do not disturb the beam in the plane normal to the plane of Fig. 1, we may consider only two spatial coordinates: z and x, along and normal to, respectively, the optical axis. We are interested in the x-dependence of the wavefunction at each point on the optical axis.

As shown earlier (Kohn & Kazimirov, 2007), the wavefunction just behind the CRL can be written as

$$\begin{aligned}\psi_0(x) &= P(x, L_s)T(x),\\ P(x, z) &= \frac{1}{(i\lambda z)^{1/2}}\exp\left(i\pi\frac{x^2}{\lambda z}\right),\\ T(x) &= \exp\left[-i\pi\frac{x^2}{\lambda F}(1-i\gamma)\right].\end{aligned} \tag{1}$$

Here $P(x, z)$ is the propagator in empty space along z, $T(x)$ is the propagator of the parabolic refractive lens, L_s is the distance between the source and the lens, λ is the X-ray wavelength, F is the lens focal length, $\gamma = \beta/\delta$, where δ is a decrement of the refraction index, and β is an index of absorption. One can see that the function $T^2(x)$ has an amplitude which can be described as a Gaussian function with a FWHM of $A_\gamma = 0.664(\lambda F/\gamma)^{1/2}$, usually referred to as the effective aperture. In most cases the real aperture of the lens is larger than A_γ and can be neglected. If this is not the case, the real aperture should be taken into account as well.

Transport of the wave from the lens to the crystal, diffraction of the wave of arbitrary shape by the crystal, and transport of the wave from the crystal to the detector can be performed *via* the plane-wave expansion of the wave $\psi_0(x)$. This approach is especially convenient for numerical calculations. We have the following relations,

$$\begin{aligned}\psi_1(x) &= \int\frac{dq}{2\pi}\psi_0(q)\widetilde{P}(q, l_1+l_2)\widetilde{P}_C(q-q_0)\exp\big[iq(x-x_0)\big],\\ \psi_0(q) &= \int dx\,\psi_0(x)\exp(-iqx),\end{aligned} \tag{2}$$

where

$$\begin{aligned}&\widetilde{P}(q, z) = \exp\left(-iz\frac{q^2}{2K}\right), \quad \widetilde{P}_C(q) = s\frac{1-\exp(i\varphi)}{R_2 - R_1\exp(i\varphi)},\\ &R_{1,2} = \frac{\sigma \pm a}{sf}, \quad f = \frac{\chi_{-h}}{\chi_h}, \quad s = K\chi_h,\\ &a = \left(\sigma^2 - s^2 f\right)^{1/2}, \quad \sigma = q\sin(2\theta_B) - i\mu_0, \quad \varphi = ad/\gamma_0.\end{aligned} \tag{3}$$

Here, $K = 2\pi/\lambda$, $\mu = K\chi_0''$, $\gamma_0 = \sin(\theta_B)$, χ_0, χ_h, χ_{-h} are the Fourier components of the crystal susceptibility, and χ_0'' is the imaginary part of the complex value χ_0. Finally, d is the thickness of the crystal plate, $q_0 = -K\varphi_0$, $x_0 = 2\varphi_0 l_2$ where φ_0 is the angular deviation from the position at which the region of the total Bragg reflection is at the center of the angular aperture of the lens. Note here that since the crystal rotates around the optical axis by the angle $2\theta_B$, the x coordinate of the function $\psi_1(x)$ is now along a different axis compared with the x coordinate of the function $\psi_0(x)$ (see Fig. 1). As one can see from (2), the intensity distribution at the detector position depends only on the total distance $l_1 + l_2$, and the exact position of the perfect crystal between the lens and the detector does not matter.

For the next step, we want to analyze how the intensity pattern changes with the position of the Bragg reflection region relative to the lens angular aperture, *i.e.* with the angle φ_0. The obvious effect is the shift of the intensity pattern as a whole by a distance x_0 which depends only on the angle φ_0 and the distance l_2. The most interesting effect occurs when the crystal dynamical diffraction region is shifted outside of the angular aperture of the lens and diffraction becomes kinematical.

If the real aperture of the lens can be neglected, the function $\psi_0(q)$ has the analytical expression

$$\psi_0(q) = \frac{g^{1/2}}{i(1-g-i\gamma)^{1/2}}\exp\left[iF\frac{q^2}{2K}\frac{1}{(1-g-i\gamma)}\right], \tag{4}$$

where $g = F/L_s$. In our case, $g \ll 1$. The amplitude of this function is a Gauss function with a FWHM of $Q = 5.90(\lambda F\gamma)^{1/2}$. It is easy to verify that $Q/K = 2^{1/2}A_\gamma/F$. If the lens is replaced by a very narrow slit as a source of divergent waves and the total distance $l_1 + l_2$ is very small then we can neglect the first two multipliers in the integral of (2). In this case the function $\psi_1(x)$ is a Fourier image of the complex amplitude of the crystal reflection and was calculated analytically (Afanas'ev & Kohn, 1971; Uragami, 1970) as a combination of the Bessel functions (see also Kohn & Kazimirov, 2007).

The same result can be obtained with the lens if $l_1 + l_2 = F/(1-g)$, *i.e.* at the focus of the lens. In this case the q-dependence of the product of the first two multipliers in (2)

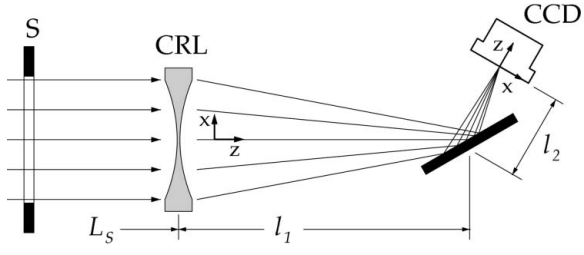

Figure 1
Experimental set-up: an X-ray wave originates from a source of finite size from far away on the left; it is restricted by the slit S, incident on the compound refractive lens CRL, and diffracted by the crystal positioned between the lens and the focus. The intensity pattern is recorded by a high-resolution CCD detector or measured by a knife edge (not shown) at the focus of the lens.

becomes very weak and is determined mostly by the absorption inside the lens. Without a crystal, from (2) we obtain a focus spot as a Gauss function with a FWHM of $2^{1/2}w_\gamma = 0.939(\lambda F\gamma)^{1/2}$ (note here that for a parabolic absorbing lens the universal relation $w_\gamma = \gamma A_\gamma$ applies). The diffraction from the crystal leads to two major effects: (i) the intensity at the focal spot extends on one side from the focus and (ii) a second peak appears which corresponds to the reflection from the back surface. The second effect takes place even in the case of the kinematical reflection when the crystal is rotated by such an angle φ_0 that $q_0 \gg Q$. Then, inside the region of integration in (2) we can use the approximation

$$P_C(q-q_0) = -\frac{s}{2q_0\sin(2\theta_B)}\left\{1-\exp\left[-i(q-q_0)2d\cos\theta_B - \mu_0 d/\cos\theta_B\right]\right\}. \quad (5)$$

Substituting (5) into (2) we can see that in the kinematical limit both sides of the crystal reflect the beam identically. In effect, the crystal reflects as two mirror surfaces spaced by a thickness d, each with a low reflectivity determined by the angular deviation from the Bragg condition. The first peak is centered at x_0 and the second peak is shifted by a distance $2d\cos\theta_B$. The relative intensity of these two peaks is determined by absorption. The peaks have the same shape as those found for the case without the crystal, *i.e.* the shape of the focused beam.

3. Experiment

The experiment was performed at the bending-magnet ESRF optical beamline BM5. The X-ray energy was tuned to 23.0 keV by using a double-crystal Si(111) monochromator. A planar parabolic refractive lens array with $N = 14$ double-concave elements each of length 102 µm with a curvature radius of $R = 6.25$ µm and aperture $A = 50$ µm (see Snigirev, Snigireva *et al.*, 2007 for details) was used to focus the X-ray beam. These lenses were manufactured using a process involving electron beam lithography and deep etching into silicon. Structures are 70 µm deep. The effective aperture was calculated as $A_\gamma = 47$ µm which was comparable with the size of the real aperture. The source-to-lens distance was $L_s = 55$ m. The focal length $F = R/(2N\delta)$ was estimated as 24.43 cm and the focus distance as 24.56 cm with an experimentally measured focus distance of 24.2 cm. The knife-edge scan shown in Fig. 2 reveals the size of the focused beam as 0.92 µm, which was limited in our experiment by the effective source size. Calculations performed for our lens and distances using the source size as the only fitting parameter (Fig. 2, solid line) gave a vertical source size of 200 µm. A more than twofold increase in the effective source size relative to the specification value was due to mechanical vibrations of the monochromator crystals. The latter value was confirmed by an independent source size measurement using the boron fiber technique (Kohn *et al.*, 2000).

The experimental set-up was assembled on a micro-optics test bench (Snigirev, Hustache *et al.*, 2007) designed for high-resolution optical characterization and equipped with precise translation and rotation stages. The crystals were mounted on a Huber circle segment with a rotation range of $\pm 15^\circ$. The X-ray intensity distribution in the focus was measured by (i) a knife-edge scan using a 200 µm Pt wire as a knife and a pin-diode as an intensity monitor, and (ii) a high-resolution CCD SensicamQE camera with 1376 × 1040 pixels, 887 µm × 670 µm field of view, and an optical pixel size of 0.645 µm. The spatial resolution of the camera was not well known; the estimation was 1.3 µm.

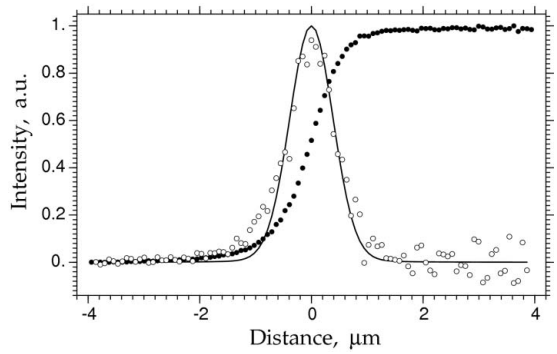

Figure 2
Beam profile at the focus spot: knife-edge scan data (solid circles), derivative (open circles) and computer simulation (solid line) for a particular type of lens used in the experiment and an effective vertical source size of 200 µm.

A perfect Si (111) oriented crystal of thickness 0.5 mm and perfect Si (111) oriented membranes produced by wet chemical etching with target thicknesses of 8 µm and 50 µm were used as samples. The 111 reflection was utilized in our experiment.

3.1. Thick silicon crystal

The knife-edge scan performed at the focus of the lens through the beam diffracted by the thick Si(111) crystal is shown in Fig. 3. The crystal was centered relative to the lens angular aperture of 180 µrad which was experimentally determined by scanning the crystal through the focused beam. This value is in good agreement with the estimation based on

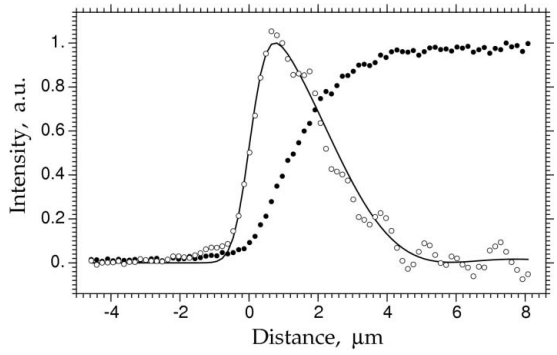

Figure 3
The shape of the focused beam (111) diffracted from the perfect bulk Si(111) crystal measured by a knife edge at the focus of the lens: raw scan data (solid circles), derivative (open circles) and the theoretical curve (solid line) were calculated by using the approach given in §2 with the vertical scaling factor used as the only fitting parameter.

A_γ and the focus distance. For comparison, the intrinsic width of the Si(111) rocking curve is 11.54 μrad. Owing to the fact that the crystal intersects only a small part of the focused X-rays, the significantly reduced intensity of the diffracted beam increases the scattering of the raw data points (solid circles in Fig. 3). To accurately calculate the derivative of the integral intensity and obtain the beam profile, the following averaging algorithm was applied,

$$\left[\frac{\mathrm{d}f(x)}{\mathrm{d}x}\right]_j = \frac{1}{h\,n(n+1)}\sum_{m=1}^{n}\left(f_{j+m} - f_{j-m}\right). \qquad (6)$$

Here, $h = 0.16$ μm is the scan step size, $n = 1$ corresponds to the standard differentiation (used to calculate the beam profile in Fig. 2) and for $n > 1$ the averaging between n points on the right and left takes place ($n = 3$ was used in analyzing the beam profile in Fig. 3). The theoretical curve was calculated using the approach given in §2, equations (1)–(3), and taking into account a source size of 200 μm determined experimentally. No fitting parameter was used except for the intensity scaling factor to compare experimental data with theory. One can see a very good agreement between the experimental profile and the theory. The highly asymmetrical shape of the peak is clearly observed and this shape reflects the physics of diffraction of a focused beam, which will be discussed in §4.

3.2. Thin silicon crystals

The spatial structure of the focused beam diffracted from thin Si membranes with thicknesses of about 8 and 50 μm were recorded using the high-resolution CCD camera. The crystal was scanned through the lens angular aperture and the images were recorded for each angular point. In this way we were able to analyze how the spatial structure of the beam changes with angle. We discovered that this pattern is different depending on whether the crystal angular Bragg diffraction region is inside or outside of the lens aperture. We have already discussed this question from a theoretical perspective; below we report the experimental results.

Beam profiles recorded from the 8 μm-thick crystal are shown in Fig. 4 for two angular positions: 35 μrad (top panel) and 140 μrad (bottom panel) from the center of the aperture. The former curve corresponds to the situation of the strong reflection, *i.e.* the maximum reflectivity is within the lens aperture. The latter curve corresponds to the situation at which the crystal is rotated outside of the angular spread of the focused beam. Two peaks are observed on both curves. The peak from the front surface on the top panel is much stronger than the second peak from the bottom surface. In the bottom panel (kinematical scattering) they are both much weaker, their intensities are almost equal, and they are narrower. The solid lines are the theoretical curves. They were calculated for the known values of the angular positions and the source size; the thickness and the resolution of the CCD camera were used as fitting parameters. Owing to the fact that the kinematical peaks are narrower and of almost the same intensity, the thickness of the crystal can be accurately determined. The fit yielded a crystal thickness of 8.67 μm and a CCD camera resolution of 1.0 μm.

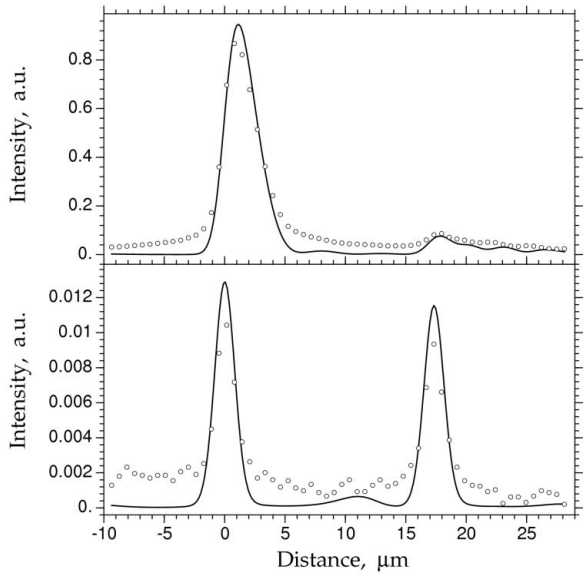

Figure 4
Spatial profiles of the focused beam (111) diffracted from the thin Si(111) membrane of target thickness 8 μm and recorded at the focus by using a high-resolution CCD camera (open circles) at different angles relative to the lens aperture. Upper panel: dynamical diffraction (the total Bragg diffraction region of the crystal is at 35 μrad from the center of the aperture). Bottom panel: kinematical diffraction (the total Bragg diffraction region is at 140 μrad from the center of the aperture). Solid lines: theoretical curves calculated for a perfect Si crystal of thickness 8.67 μm, experimentally measured source size and a camera resolution of 1.0 μm.

Experimental results from the 50 μm-thick crystal are shown in Fig. 5 for the same angular positions: 35 μrad from the center of the aperture (top panel, dynamical diffraction)

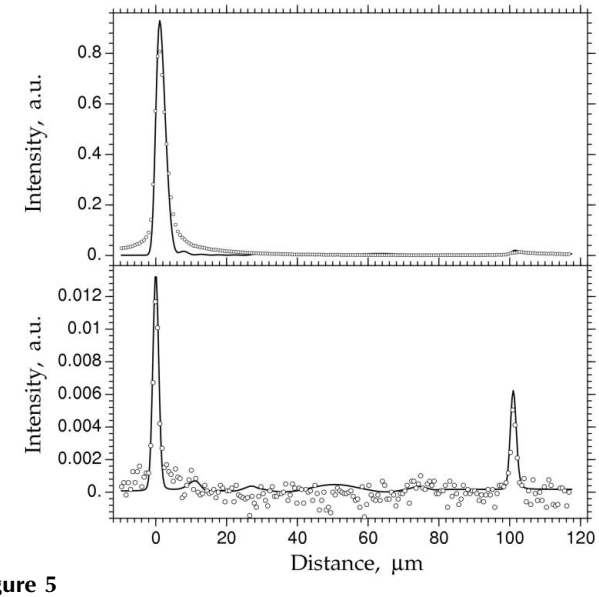

Figure 5
Same as in Fig. 4 but for the Si membrane of target thickness 50 μm. Solid lines: theoretical curves calculated for a perfect Si crystal of thickness 50.54 μm, experimentally measured source size and a camera resolution of 1.0 μm.

and 140 μrad (bottom panel, kinematical diffraction). The peak from the back surface is hardly seen in the dynamical regime compared with the peak from the front surface, while in the kinematical case the intensity of this peak is about half of the intensity of the front peak. As for the previous sample, the kinematical peaks are noticeably narrower. The solid lines are the best fit yielding a crystal thickness of 50.54 μm and a camera resolution of 1.0 μm; they were calculated for fixed values of the source size and angular positions of the crystal relative to the lens angular aperture.

4. Discussion

We want first to discuss the results obtained from the thick crystal and turn our attention again to Fig. 3. As we mentioned earlier, the asymmetrical shape of the beam profile has a clear physical explanation. According to the theory, the left side of the peak should be as sharp as the incident beam in the focus. Our results confirm that the left side follows the profile of the focus spot shown in Fig. 2 which, in our particular case, is the image of the source. The slope on the right side of the peak is determined by the extinction effect. The extinction length is the depth below the crystal surface at which the amplitude of the plane wave is attenuated e times, and at the center of the angular region of the total reflection it is equal to $L_{ex} = 2\sin\theta_B/(K|\chi_h|)$ (Kohn, 2002). The X-ray reflected from this depth is shifted by a distance $x_{ex} = 2L_{ex}\cos\theta_B$; in our case $x_{ex} =$ 3.06 μm. The extinction effect is one of the most fundamental consequences of dynamical diffraction. Thus, our set-up offers a unique opportunity to visualize the extinction length in crystals. Note that the broadening of a very narrow beam by the extinction effect in the space domain described here is analogous to the broadening of a very short X-ray pulse in the time domain (Wark & He, 1994; Chukhovskii & Förster, 1995).

Let us now turn to the spatial patterns recorded from the thin crystals. The second peak in the diffraction pattern which originates from the back surface of a sufficiently thin crystal was predicted theoretically in the 1970s for an infinitely narrow beam (Afanas'ev & Kohn, 1971; Uragami, 1970); it was discussed in detail for a beam focused by a refractive lens (Kohn, 2006; Kohn & Kazimirov, 2007), and reported recently by analyzing a virtual diffraction from an angular aperture (Yan *et al.*, 2008). Back-reflection images as dynamical diffraction artifacts were considered theoretically and studied experimentally by using a narrow X-ray beam produced by a 50 μm-wide slit (Yan & Noyan, 2005). Reflections from the back surfaces were observed experimentally on strained silicon-on-insulator layers by using a 200 nm beam produced by a circular Fresnel zone plate (Kazimirov *et al.*, 2008, 2009). In this work, by using perfect thin crystals we have an opportunity to perform a detailed comparison of theory with experiment. Given that the theoretical curves in Figs. 4 and 5 were calculated by using only two variables, the thickness of the crystals and the spatial resolution of the CCD camera (the same value was used for all curves), we may conclude that the agreement is very good and the theory is capable of predicting fine details of the spatial pattern.

By analyzing the CCD images recorded at different angles of the crystal relative to the angular aperture of the lens we discovered dramatic changes in the diffraction pattern. At angles at which the maximum crystal reflectivity is within the angular aperture (top curves in Figs. 4 and 5), the peak from the front surface dominates and almost all intensity originates from the layer located at the surface of the crystal within the extinction depth. As the scan proceeds and the maximum reflectivity shifts outside of the lens angular aperture the situation changes. For the 8 μm-thick crystal the two peaks are almost equal in intensity, and for the 50 μm-thick crystal the peak from the front surface is only about two times stronger. The difference in intensity is now determined by absorption. The kinematical peaks are narrower; their width is almost equal to the size of the incident beam, and in our experiments is determined by the spatial resolution of the detector. This observation reflects the fact that the depth of the layer participating in kinematical diffraction is very small and its value is inversely proportional to the angular deviation from the Bragg angle. By using extremely small beams and performing knife-edge scans it becomes feasible to experimentally measure the thickness of the scattering layer as a function of angle.

It has already been pointed out that dynamical artifacts in the form of the back-reflected images have to be considered in analyzing experiments with narrow beams (Yan & Noyan, 2005). Our results help to shed light on the origin of the diffracted intensity in a microbeam diffraction experiment. In a typical experiment the intensity is recorded by a detector located far away from the focus at a typical distance of about 1 m and, even if recording on a CCD detector, all spatial features are washed out. One may be tempted to attribute all measured intensity as originating from the illuminated volume as a whole. As we can see from our results, this is not the case. Moreover, the contribution from different depths changes with angle. Of course, this is true only for perfect crystals which are not very often the subject of experimental analysis. However, one should consider two points. Firstly, the experimental results show that even for not very perfect strained layers the contribution from the surface layer within the extinction length is much stronger than that from the bulk underneath (Kazimirov *et al.*, 2008, 2009). Secondly, we may expect that for a real mosaic crystalline sample a focused beam of size much smaller than the grain size positioned within an individual grain diffracts from a more regular lattice than a macrobeam diffracting from many grains and grain boundaries.

5. Conclusion

By using refractive lenses as focusing optics and perfect silicon crystals of different thickness as model samples we studied the spatial structure of the focused beam diffracted from crystals and performed a detailed comparison with theory. If the maximum reflectivity is within the angular aperture, we observed the asymmetric shape of the diffracted beam. In the case of a thick perfect crystal the asymmetry is due to the

extinction effect. Our set-up offers a unique possibility to visualize the extinction length in crystals. For thin crystals, we studied the evolution of the spatial structure as the crystal is scanned through the angular aperture of the lens. If the maximum reflectivity is within the angular aperture the peak from the front surface is much stronger than the peak from the back surface of the crystal. If the maximum reflectivity is outside of the angular aperture, both surfaces effectively reflect as mirrors with reduced reflectivity. The peaks are narrow, approaching the width of the focused beam. By using a sufficiently small beam it becomes possible to experimentally measure the thickness of the scattering layer as a function of angle. The use of much smaller beams in future experiments may reveal new finer details in the spatial structure that theory predicts and which we were not able to resolve in this first experiment.

This work is based upon research conducted at the Cornell High Energy Synchrotron Source (CHESS) which is supported by the National Science Foundation and the National Institutes of Health/National Institute of General Medical Sciences under NSF award DMR-0225180. The work of VGK was supported by RFBR Grant Nos. 07-02-00067a and RS-4110.2008.2. We acknowledge the European Synchrotron Radiation Facility for provision of synchrotron radiation facilities and we would like to thank the ESRF staff for assistance in using beamline BM5.

References

Afanas'ev, A. M. & Kohn, V. G. (1971). *Acta Cryst.* A**27**, 421–430.
Chukhovskii, F. N. & Förster, E. (1995). *Acta Cryst.* A**51**, 668–672.
Kazimirov, A., Kohn, V. G. & Cai, Z.-H. (2008). *Proc. SPIE*, **7077**, 70770L.
Kazimirov, A., Kohn, V. G. & Cai, Z.-H. (2009). *J. Phys. D*, **42**, 012005.
Kohn, V. G. (2002). *Phys. Status Solidi B*, **231**, 132–148.
Kohn, V. G. (2003). *J. Exp. Theoret. Phys.* **97**, 204–215.
Kohn, V. G. (2006). *Crystallogr. Rep.* **51**, 564–569.
Kohn, V. G. & Kazimirov, A. (2007). *Phys. Rev. B*, **75**, 224119.
Kohn, V., Snigireva, I. & Snigirev, A. (2000). *Phys. Rev. Lett.* **85**, 2745–2748.
Michette, A. G. (1986). *Optical Systems for Soft X-rays.* New York/London: Plenum.
Snigirev, A., Hustache, R., Duboc, P., Massonnat, J.-Y., Claustre, L., Van Vaerenbergh, P., Snigireva, I., Grigoriev, M. & Yunkin, V. (2007). *Proc. SPIE*, **6705**, 670511.
Snigirev, A., Kohn, V., Snigireva, I. & Lengeler, B., (1996). *Nature (London)*, **384**, 49–51.
Snigirev, A., Snigireva, I., Grigoriev, M., Yunkin, V., Di Michiel, M., Kuznetsov, S. & Vaughan, G. (2007). *Proc. SPIE*, **6705**, 670506.
Uragami, T. S. (1970). *J. Phys. Soc. Jpn*, **28**, 1508–1527.
Wark, J. S. & He, H. (1994). *Laser Part. Beams*, **12**, 507–513.
Yan, H., Kalenci, Ö., Noyan, I. C. & Mase, J. (2008). *J. Appl. Phys.* **104**, 023506.
Yan, H. & Noyan, I. C. (2005). *J. Appl. Phys.* **98**, 073527.